International Journal of Precision Engineering and Manufacturing-Green Technology
https://doi.org/10.1007/s40684-026-00908-3
Online ISSN 2198-0810

REGULAR PAPER

Geometry-Sensitive Fatigue Behavior of Ultra-Thin Copper-Brazed 316 L STS Joints: Experimental Characterization and Stress-Life Analysis

Melkamu Tadesse Getachew[1] · Hong Seok Kim[2] · Seokyoung Ahn[3] · Sang Hu Park[3]

Received: 28 January 2026 / Revised: 18 April 2026 / Accepted: 2 June 2026

Abstract
The fatigue reliability of plate heat exchangers (PHEs) is increasingly governed by brazed joints as ultra-thin stainless steel (STS) plates are adopted to enhance efficiency. However, the peel-mode fatigue behavior of copper-brazed joints, particularly under conditions combining ultra-thin geometry, micro-scale fillet features, and Mode-I loading, remains largely unexplored. This study presents a systematic characterization of peel fatigue in 316 L (50 μm)–Cu (12 μm)–316 L (50 μm) brazed joints through an integrated experimental and finite element framework. Two distinct fatigue regimes were identified: high-cycle fatigue (50–100 N; 10^4-10^5 cycles) characterized by stable crack growth within the copper layer, and low-cycle fatigue (150–200 N; 10^3-10^4 cycles) dominated by plastic deformation and accelerated crack initiation. Three crack propagation modes were observed, with copper-confined propagation dominating at lower loads. Finite element analysis considering fillet radii of 4–9 μm revealed a strong geometry-dependent stress response, where local stress increased from 205 to 217 MPa (6%) near yield conditions and from 448 to 580 MPa (30%) in the plastic regime as fillet radius decreased. A geometry-sensitive stress–life framework was developed by combining finite element stress mapping with experimental force–life data, demonstrating that stress-based evaluation captures fillet effects not evident in force-based analysis. These results provide quantitative design guidance by linking fillet geometry control to fatigue reliability of ultra-thin brazed joints in lightweight thermal systems.

AQ1

Highlights

- As authors know, it is the first systematic peel fatigue characterization of ultra-thin (50 μm) Cu-brazed 316 L STS joints.
- Geometry-sensitive stress vs. life linking microscale fillet radius to fatigue performance.
- Identification of three distinct crack propagation modes governed by the end of joint morphology (fillet shape's uniformity).
- Quantitative evidence that fillet radius influence is strongly load-dependent (6% vs. 30% stress increase).

Keywords Ultra-thin brazed joints · Peel-mode fatigue · Fillet radius · Stress–life framework · Finite element analysis · Plate heat exchanger

✉ Sang Hu Park
sanghu@pusan.ac.kr

[1] Graduate School of Mechanical Engineering, Pusan National University, Busandaehak-ro, Busan 46241, Republic of Korea

[2] Research Institute of Mechanical Technology, Pusan National University, Busandaehak-ro, 46241 Busan, Republic of Korea

[3] School of Mechanical Engineering, Pusan National University, Busandaehak-ro, 46241 Busan, Republic of Korea

1 Introduction

AQ2

Plate heat exchangers (PHEs) are critical components in modern thermal management systems, serving applications from HVAC and chemical processing to nuclear power plants and hydrogen production facilities [1–5]. Their compact geometry, high surface-area-to-volume ratio, and ability to withstand cyclic thermo-mechanical loading make them essential for high-efficiency, long-service-life applications [6–8]. Typical PHEs comprise multiple thin stainless

Published online: 01 July 2026

steel (STS) sheets that are embossed and metallurgically bonded to form alternating flow channels [9–11]. The use of thin and ultra-thin sheets enables lightweight structures, reducing material consumption while enhancing heat transfer efficiency, which is important for energy-efficient thermal systems [7, 8].

Copper-filler brazing has been considered as a predominant joining method for stainless steel PHEs due to its excellent wettability, rapid capillary infiltration, and reliable bonding under vacuum conditions [10, 12–16]. However, despite these processing advantages, the brazed joint remains the most vulnerable region owing to thermal expansion mismatch, cooling-induced residual stresses, and filler to base metal interactions (ex. intermetallic compound layer) [16–19]. Till now, various research works have demonstrated that joining processes fundamentally degrade mechanical performance at bonded interfaces, reducing yield strength, fracture toughness, and fatigue life compared to the base metal [20–26]. The trend toward thinner plates to enhance thermal performance has increased susceptibility to fatigue cracking at joints, fillets, and stress concentrations [27–38]. During industrial operation, PHE plates experience repeated pressure pulsations, temperature gradients, flow-induced vibrations, and repetitive loading cycles [2, 6, 23].

Recent studies on the fatigue behavior of brazed joints in PHE applications can be broadly categorized into three groups. First, material-focused fatigue studies, such as Hanželič et al. [10] and Hayta and Kandemir [16], have investigated fatigue performance under uniaxial or strain-controlled loading, primarily aiming at material selection and lifetime prediction. However, these studies are conducted on relatively thick plates (≥ 0.4 mm) and focus on bulk material response, without resolving local stress concentration effects at the joint scale. Second, geometry-oriented investigations, such as Jöckel et al. [39], have examined the influence of brazing process parameters and fillet geometry on fatigue strength under shear and peel loading. While these works highlight the importance of local geometry, they are limited to millimeter-scale fillet radii and defect-driven failure mechanisms, which differ fundamentally from ultra-thin, defect-minimized joints. Third, structural-level analyses, such as Ma et al. [37], have evaluated fatigue behavior using finite element approaches based on structural parameters and thermal cycling conditions. However, these studies do not capture the local crack initiation mechanisms and geometry-driven stress concentration at the micro-scale fillet region.

Table 1 Comparison of fatigue studies on copper-brazed STS joints

References	Material	Plate Thickness	Cu Filler	Loading Mode	Fatigue Life Range
Hanželič et al. [10]	316L STS	Not specified	37 µm	Uniaxial tension	10^5~10^6 (HCF)
Hayta et al. [16]	316L/304L STS	0.4 mm	50 µm	Strain-controlled	10^3~10^5
Jöckel et al. [39]	X5CrNi18-10	2.0 mm	Cu 110	Peel/Shear	10^4~10^6
Ma et al. [37]	Al alloy	1.0 mm	Al-Si	Thermal cycle	~10^3 (LCF)
This work	316L STS	50 µm	12 µm	Peel (Mode-I)	10^3~10^5

Despite these efforts, a critical gap remains in understanding fatigue behavior at the ultra-thin scale (~ 50 µm). At this scale, both material size effects and geometric scaling of fillet features become dominant. Micro-scale studies on copper foils [30] have shown that mechanical behavior deviates significantly from bulk response below ~ 75 µm thickness, indicating that conventional fatigue models may not be directly applicable. More importantly, existing studies do not simultaneously address three key aspects: (i) ultra-thin sheet thickness, (ii) micro-scale fillet geometry (µm-level), and (iii) peel-mode (Mode-I) loading, which governs crack initiation in PHE joints. This limitation is clearly demonstrated in Table 1, which compares representative fatigue studies on brazed joints.

Previous investigations have been restricted to conventional plate thicknesses (0.4–2.0 mm) and relatively thick filler layers (37–110 µm), with loading conditions dominated by uniaxial tension or shear. None of these studies simultaneously considers ultra-thin sheets, thin interlayers (~12 µm), and peel-mode loading, which are critical for realistic PHE failure conditions. The present study addresses this gap by investigating a fundamentally different regime involving 50 µm 316 L sheets with a 12 µm copper interlayer under peel-mode loading, which more accurately represents the Mode-I crack-driving forces at brazed joint fillets during pressure cycling. To the best of the authors' knowledge, fatigue behavior under this combined set of conditions has not been systematically examined.

Conventional mechanical testing configurations fail to replicate PHE failure conditions. Standard lap-shear tests (ASTM D1002) introduce bending moments and mixed-mode stresses that obscure interfacial behavior, particularly in ultra-thin sheets prone to edge tearing [40]. Previous studies have shown that fatigue failure in brazed joints is governed by Mode-I opening at the fillet rather than nominal shear stress [12, 16, 30]. This distinction is schematically illustrated in Fig. 1, which contrasts conventional test configurations (axial tension and lap-shear) with peel-mode loading that directly represents the crack-driving mechanism at brazed fillets. As shown, only the peel configuration isolates the Mode-I opening condition relevant to PHE service environments.

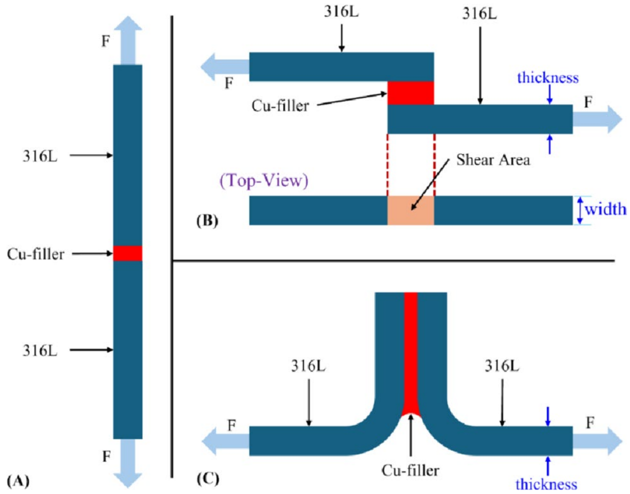

Fig. 1 Schematic diagrams of brazed joint test methods: (**A**) butt-jointed axial tension, (**B**) lap jointed shear, and (**C**) peel mode representing Mode-I opening at the fillet

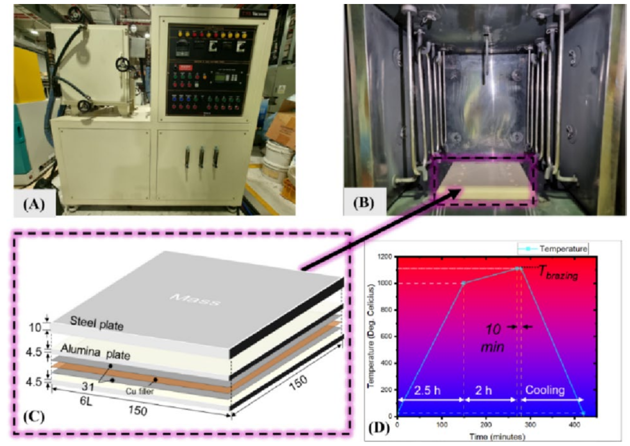

Fig. 2 Brazing procedure: (**a**) vacuum brazing machine, (**b**) chamber interior, (**c**) specimen stacking configuration with alumina plates and steel mass, and (**d**) temperature control profile

Furthermore, while Jöckel et al. [39] demonstrated that crack initiation occurs within the first third of the fillet radius in conventional-thickness specimens, no study has quantified how micro-scale fillet geometry interacts with ultra-thin sheet mechanics to govern fatigue behavior. The fillet radii in their study (0.26–2.76 mm) are orders of magnitude larger than those in ultra-thin joints (4–7 µm in the present study), suggesting fundamentally different stress concentration mechanisms.

This study develops an integrated experimental and numerical framework to characterize the peel-mode fatigue behavior of ultra-thin 316 L (50 µm)–Cu (12 µm)–316 L (50 µm) brazed joints. It specifically addresses the combined effects of ultra-thin sheet thickness, micro-scale fillet geometry, and peel-mode loading. The specific objectives are to: (i) characterize joint morphology and fillet geometry through microstructural analysis; (ii) establish monotonic and cyclic peel response through systematic mechanical testing; (iii) develop and validate a finite element model capturing local stress states at the fillet; (iv) construct geometry-sensitive stress–life curves quantifying the effect of fillet radius; and (v) compare the results with existing literature to elucidate thickness-dependent fatigue mechanisms.

2 Materials and Methods

2.1 Materials and Brazing Procedure

In this study, ultra-thin 316 L stainless steel (STS) sheets with a thickness of 50 µm and pure copper filler foil with a thickness of 12 µm were used. The chemical composition of the 316 L sheets is listed in Table 2.

The vacuum brazing machine shown in Fig. 2(a) was used for the brazing process in this study. Prior to brazing, the stainless steel sheets and copper filler were stacked between alumina plates, and a steel mass was placed on top to ensure uniform contact and alignment during heating, as illustrated in Fig. 2(c). This configuration was used to produce brazed multilayer sheets for material property determination, which were later used in tensile testing for inverse calibration of the copper interlayer properties. The assembled stack was then placed inside the furnace chamber, shown in Fig. 2(b), for brazing.

Brazing was carried out under a vacuum level of approximately 7×10^{-3} Torr. The brazing temperature control profile is presented in Fig. 2(d) and follows the procedure reported by Kim et al. [15]. The specimens were first heated from room temperature to 1000 °C over approximately 2.5 h, followed by heating to the brazing temperature of 1110 °C within 2 h. The temperature was then held at 1110 °C for 10 min to ensure complete melting and capillary infiltration of the copper filler between the stainless steel sheets. After the holding stage, the specimens were cooled inside the furnace under vacuum conditions to room temperature.

Table 2 Chemical composition of 316 L stainless steel (wt%)

Element	Fe	Cr	Ni	Mo	Mn	Si	C	*P*	S
316 L	Bal.	16–18	12–15	2–3	< 2	< 1	< 0.03	< 0.045	< 0.03

The materials used in this study represent the thinnest STS plate and Cu filler (12 µm) compared with those reported in previous works [10, 16], corresponding to the lower bound of materials considered for lightweight plate heat exchanger (PHE) applications. A separate specimen configuration was used for peel and cyclic peel fatigue testing, as shown in Fig. 3(A). After brazing, the required test specimens for both tensile (opening mode) testing and peel fatigue experiments were extracted from the brazed plates by wire cutting, as illustrated in Fig. 3(B).

2.2 Microstructural Characterization

Optical microscopy (OM) was used to assess copper layer uniformity, confirm metallurgical bonding, and verify the absence of voids (Fig. 3C). Unlike previous studies that reported initial defects and crack-like cavities in conventional brazed joints [39], the ultra-thin joints in this study exhibited continuous bonding without visible defects. OM imaging enabled visualization of copper infiltration and fillet formation, providing geometric boundary conditions for FE modeling.

2.3 Monotonic and Cyclic Peel Testing

The peel behavior of the brazed joints was evaluated through monotonic and cyclic loading tests. Monotonic peel tests were performed using a 2-ton universal testing machine under displacement control at a constant crosshead speed of 2 mm/min. Tests were conducted on five specimens at room temperature. The specimen geometry and dimensions consisted of a centrally located brazed interface flanked by unbonded 316 L tabs (Fig. 3-D), enabling stable gripping while maintaining a pure Mode-I (opening) loading condition. All tests were conducted using a fixture designed to promote Mode-I delamination (Fig. 3-E), thereby minimizing bending and shear-induced failure. Prior to testing, specimens were carefully aligned to avoid eccentric loading, and a small pre-load (~1.5 N) which is less than 1% of maximum load was applied to ensure stable contact in the grips. Force was measured using the machine's calibrated load cell, and force–displacement data were continuously recorded.

Cyclic peel tests were conducted under load-controlled loading (R = 0.1) to characterize fatigue resistance. The loading levels were selected based on the monotonic response and prior literature [10, 16, 39] to capture both sub-yield and near-/above-yield regimes. For low-cycle fatigue (LCF), 14 specimens were tested at maximum loads of 150, 175, and 200 N with a frequency of 0.3 Hz (Fig. 4-A), representing high-amplitude loading with significant damage accumulation per cycle. The grip configuration, pre-loading, and post-test conditions are illustrated in Fig. 4-A (labels 1–3). For high-cycle fatigue (HCF), 8 specimens were tested at maximum loads of 50, 75, and 100 N with a frequency of 10 Hz using a servo-hydraulic testing system (Fig. 4-B), corresponding to lower stress amplitudes with a large number of cycles. During cyclic testing, displacement evolution and number of cycles were continuously recorded. For each loading level, multiple specimens (2–3) were evaluated to ensure repeatability.

2.4 Material Property Determination

Uniaxial tensile tests were performed on specimens extracted from brazed sheets (Fig. 5). Because the copper interlayer thickness is only ~12 µm and is confined between stainless steel sheets, direct mechanical testing of the filler

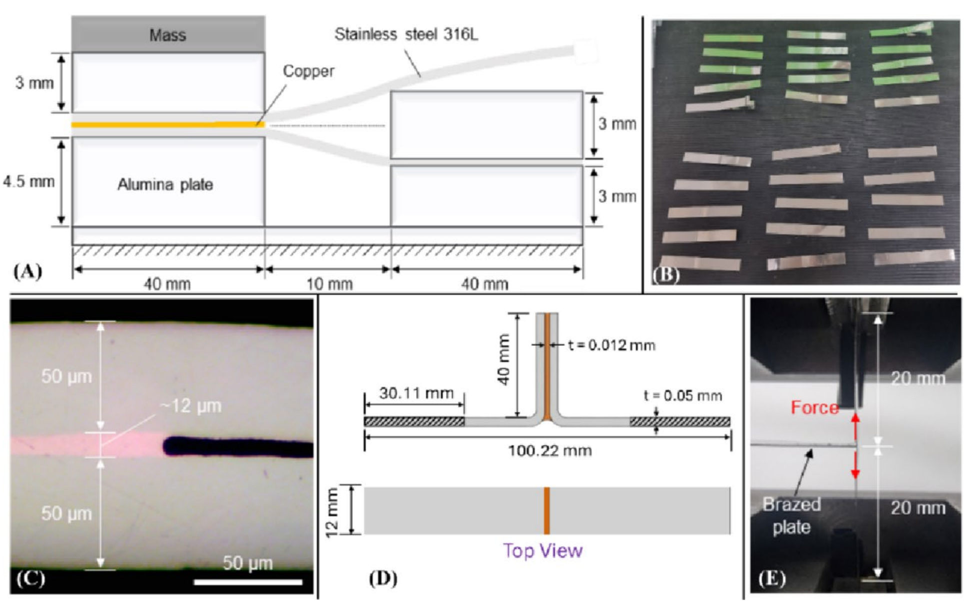

Fig. 3 (**A**) Specimen preparation and jig orientation prior to brazing (thickness direction view), (**B**) brazed specimens after wire cutting (top view), (**C**) optical micrograph of the 316 L–Cu–316 L brazed joint cross-section (thickness direction), (**D**) specimen dimensions, and (**E**) gripped specimen during testing

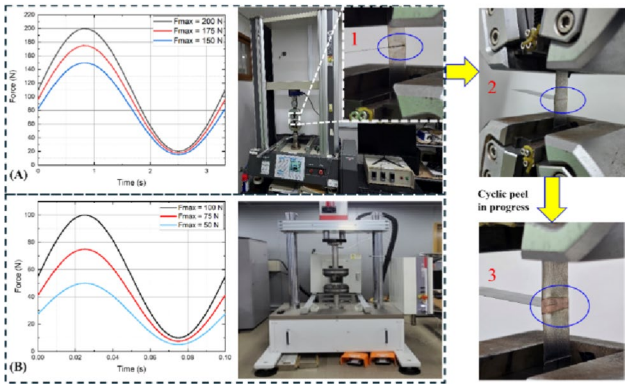

Fig. 4 Experimental setups for fatigue testing: (**A**) low-cycle fatigue configuration showing grip arrangement (1), pre-loading (2), and post-test condition (3); (**B**) high-cycle fatigue configuration with servo-hydraulic system (a tensioned specimen is shown in the blue circle)

material alone is experimentally infeasible. Therefore, the copper interlayer properties were determined through an inverse calibration procedure based on the experimentally measured force–displacement response of the brazed multilayer specimens.

The inverse calibration workflow, illustrated in Fig. 6, employed literature-based stress–strain data for pure copper [41] as the initial estimate (PS#0). Iterative FE simulations were then performed until the simulated force–displacement response converged with the experimental results. The optimized copper behavior was represented by an exponential constitutive model:

$$\sigma = A \cdot exp\left(-\varepsilon/C\right) + B \cdot exp\left(-\varepsilon/D\right) + E \tag{1}$$

where, σ is effective stress and ε is effective strain. Parameter Set 2 (PS#2) (A=−140.5 MPa, B=−1254 MPa, C=0.00774, D=0.55922, E=1486 MPa) was selected based on validation against experimental data (see Fig. 7).

The copper constitutive parameters used in the FE simulations were determined through inverse calibration using experimentally measured force–displacement responses of brazed 316 L–Cu–316 L multilayer specimens. Because these calibration specimens had already undergone the

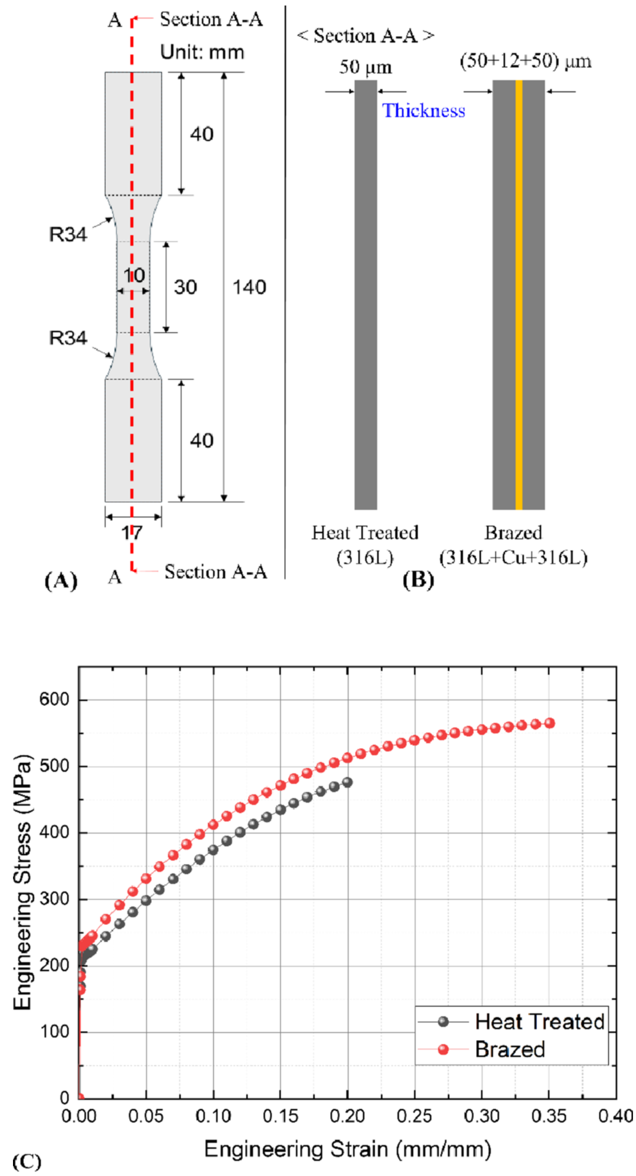

Fig. 5 Tensile specimen: (**A**) design geometry, (**B**) cross-sectional view of 50-12-50 μm multilayer structure, and (**C**) engineering stress–strain comparison between heat-treated 316 L and brazed 316 L-Cu-316 L plates

Fig. 6 Inverse calibration workflow for determining effective copper filler properties: Step 1 provides input data; Step 2 performs FE simulation; Step 3 validates predicted vs. experimental force–displacement curves; iteration continues until convergence

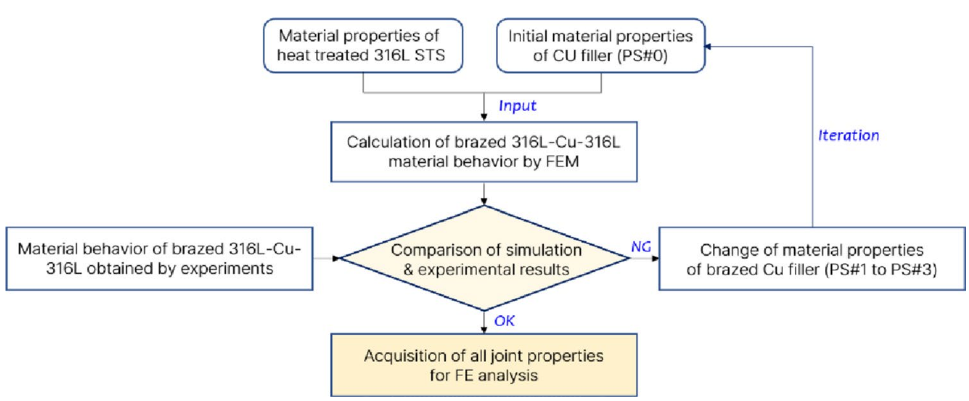

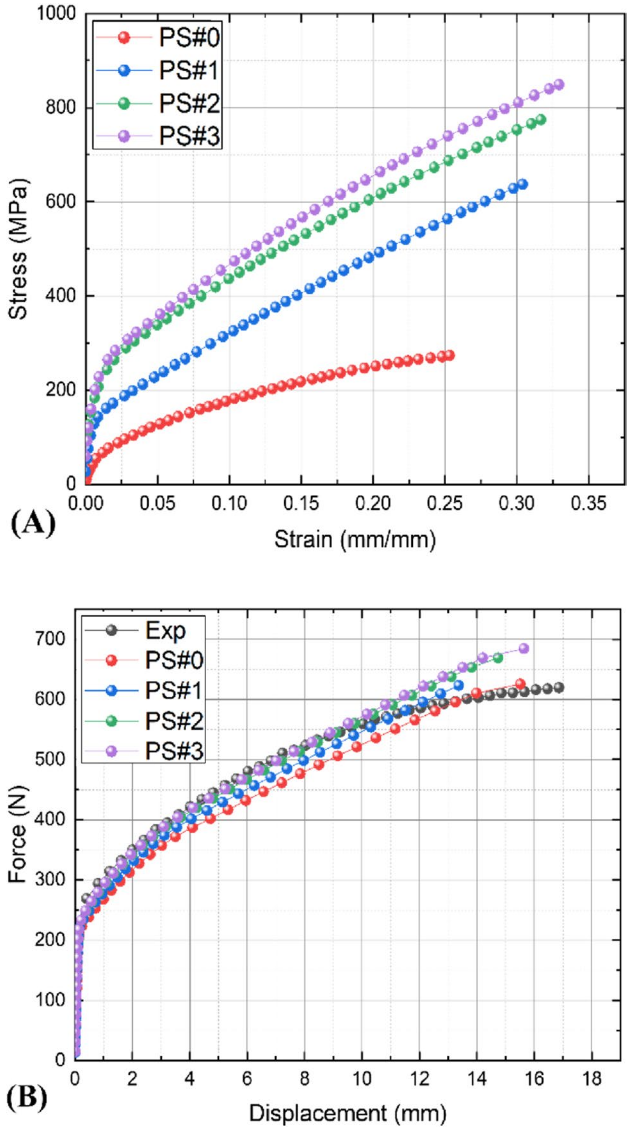

Fig. 7 (**A**) Stress–strain behaviors of copper with different parameter sets, (**B**) validated force–displacement comparison with experimental data

complete brazing thermal cycle and cooling, the calibrated parameter set reflects the effective mechanical behavior of the copper interlayer in the post-brazing condition, including microstructural changes induced by the brazing process. Since the calibration was performed using a single multilayer specimen configuration, the parameters should be interpreted as an effective constitutive representation of the copper interlayer for the present joint configuration.

2.5 Finite Element Modeling

FE simulations were performed using ANSYS 2025 (Static Structural, ANSYS Inc., Canonsburg, PA, USA). The finite element model was constructed using a two-dimensional plane-strain formulation to represent two 50 µm thick 316 L stainless steel sheets bonded by a 12 µm copper interlayer. The plane-strain assumption was adopted because the specimen width in the experiments (12 mm) is significantly larger than the sheet thickness (50 µm), corresponding to a width-to-thickness ratio of approximately 240. The displacement boundary conditions were applied to replicate the experimental peel configuration. One end of the lower sheet was fully constrained, while a vertical displacement was applied to the upper sheet to induce Mode-I opening. The interface between the stainless steel and copper interlayer was assumed to be perfectly bonded, consistent with the defect-free joints observed experimentally. As illustrated in Fig. 8(B), a refined mesh was employed in the fillet region to accurately capture stress concentration effects, while a coarser mesh was used in regions away from the interface to reduce computational cost. A mesh convergence study was conducted to ensure that the predicted stress values were independent of mesh size.

Optical microscopy observations revealed that the copper fillet geometry in the brazed joints typically falls within the range of approximately 8.9–13 µm (fillet diameters), and

Fig. 8 (**A**) Fillet geometry variations (R=4, 6, 7, and 9 µm) considered in FE modeling, (**B**) mesh distributions and representative stress distribution (R=9 µm) during peel delamination

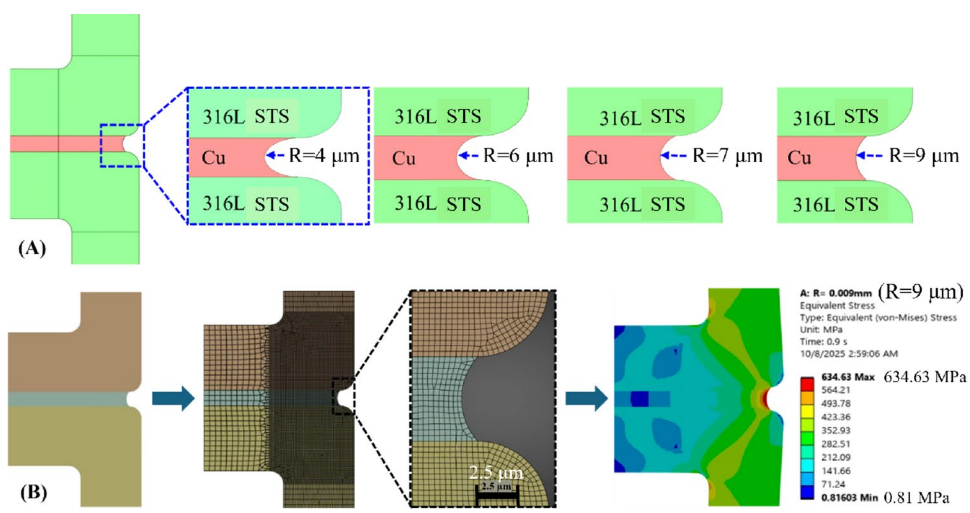

the radii (R) used in the FE simulations as shown in Fig. 8(A) ($R = 4$, 6, 7, and 9 µm), were therefore selected as representative values within this micro-scale geometric range to investigate stress sensitivity to fillet morphology. Notably, these radii are one to two orders of magnitude smaller than the fillet radii reported for conventional brazed joints (0.26–2.76 mm) by Jöckel et al. [39], highlighting the fundamentally different geometric scale associated with ultra-thin joints.

Thermally induced residual stresses generated during the brazing thermal cycle were not explicitly considered in the present FE analysis. The sheets used in this study are extremely thin (50 µm stainless steel with a 12 µm copper interlayer) and were not rigidly constrained during vacuum furnace brazing. As a result, the structure exhibits high compliance, allowing deformation and stress relaxation during cooling rather than accumulation of significant residual stresses. In addition, brazing was performed under uniform furnace heating conditions, minimizing temperature gradients within the assembly. Therefore, the present analysis focuses on the mechanical stress concentration induced by fillet geometry under peel loading. Furthermore, the copper interlayer properties used in the FE model were calibrated using experimental responses of brazed multilayer specimens, ensuring representation of the effective post-brazing mechanical behavior of the joint system.

The applied loading conditions and boundary constraints were defined to be consistent with the experimental peel tests, ensuring direct comparability between the simulated stress distribution and experimentally observed fatigue behavior.

3 Results

3.1 Joint Morphology and Fillet Geometry

Figure 9(A) shows representative optical micrographs revealing continuous copper filler across the joint. Despite nominal 12 µm thickness, local fillet diameter varied from ~ 8.9 to 13.0 µm, corresponding to fillet radii of approximately 4 to 7 µm. FE-SEM and EPMA analysis (Fig. 9B) confirmed a well-defined Cu-rich interlayer with limited interdiffusion. Importantly, unlike the crack-like initial defects (up to 0.4 mm depth) reported in conventional brazed joints by Jöckel et al. [39], no such defects were observed in the ultra-thin joints, indicating that the manufacturing process produced higher-quality bonding at this scale.

This defect-free morphology ensures that the observed fatigue behavior is governed primarily by geometry and stress concentration effects rather than manufacturing-induced defects, enabling clearer interpretation of intrinsic fatigue mechanisms.

3.2 Monotonic Peel Response

Figure 10 compares experimental and FE-predicted monotonic peel responses. Experimental curves show yielding at ~ 82 N followed by stable propagation under Mode-I loading. The FE model reproduces initial stiffness and overall trends with predicted yield at ~ 84 N, validating the calibrated material properties.

This agreement indicates that the calibrated copper interlayer properties effectively capture the mechanical response of the brazed joint under Mode-I loading. The

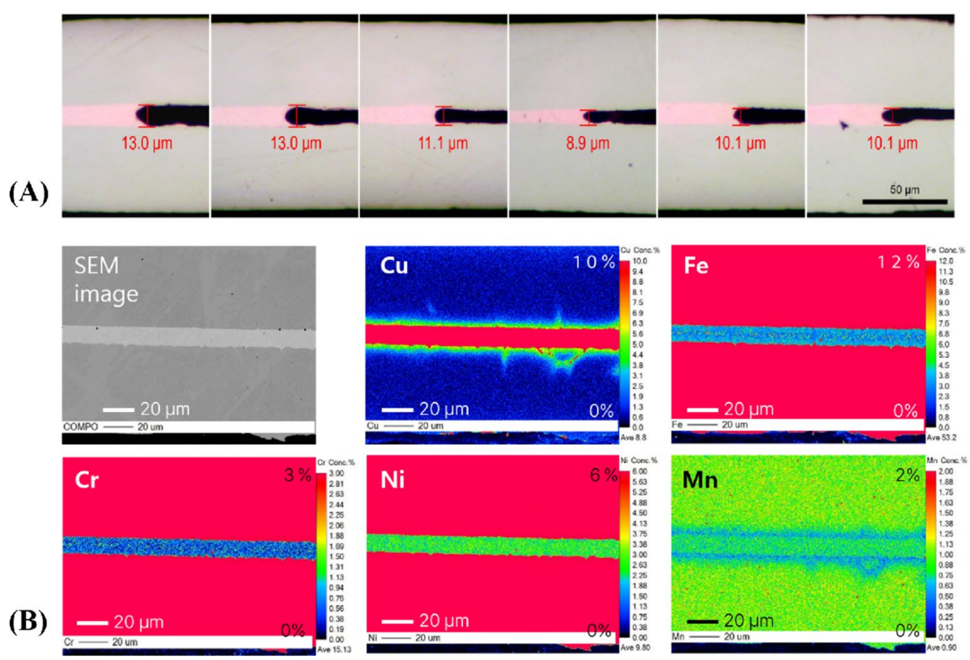

Fig. 9 (**A**) Optical micrographs showing fillet thickness variation (from about 8.9 to 13.0 µm), (**B**) FE-SEM and EPMA elemental maps confirming Cu-rich interlayer with limited interdiffusion

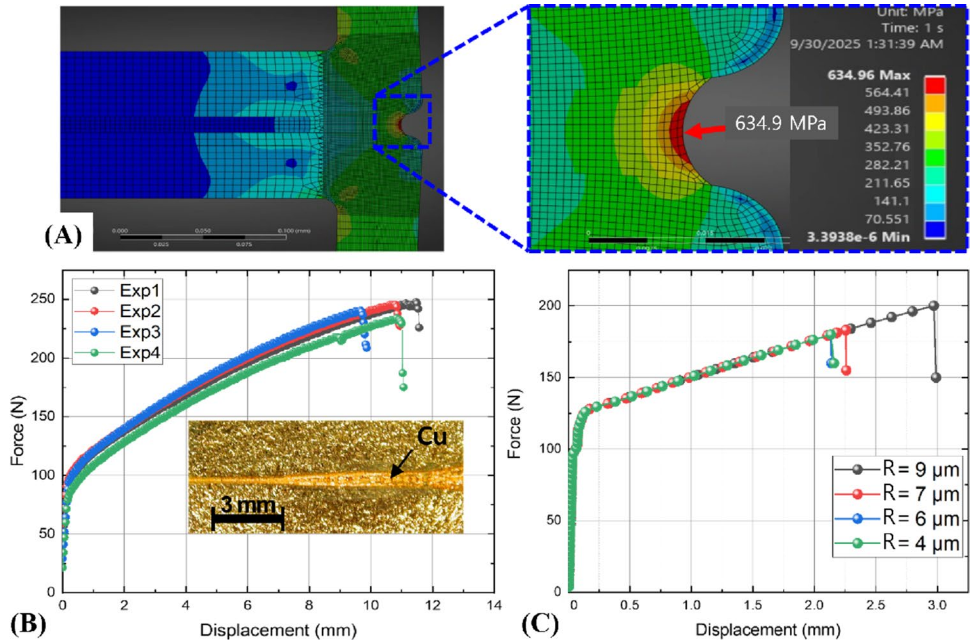

Fig. 10 (**A**) FE model mesh configuration, (**B**) experimental force–displacement curves showing yield at ~82 N, (**C**) simulated response with yield at ~84 N validating calibrated properties

stable post-yield behavior suggests that crack propagation is governed by continuous plastic deformation within the copper layer rather than abrupt interfacial failure, which is consistent with the defect-free joint morphology observed in Fig. 9.

Figure 11 summarizes cyclic peel fatigue behavior. Fatigue life data reveal a strong inverse relationship between maximum force and cycles to failure. HCF lives ranged from ~ 44,000–141,000 cycles at 50–100 N, while LCF lives decreased to ~ 2,800–22,000 cycles at 150–200 N. These fatigue life ranges are comparable to those reported by Hayta and Kandemir [16] for strain-controlled testing of 0.4 mm thick plates (10^3–10^5 cycles), suggesting similar damage accumulation rates despite the different loading modes and geometric scales. This trend can be attributed to the increasing contribution of plastic deformation at higher load levels. In the HCF regime, deformation is relatively limited, allowing gradual damage accumulation and longer fatigue life. In contrast, in the LCF regime, elevated stress levels intensify local plastic deformation at the fillet, accelerating crack initiation and propagation. This behavior highlights the strong sensitivity of ultra-thin joints to local stress concentration under Mode-I loading.

The HCF dataset consists of eight specimens distributed across three load levels (50, 75, and 100 N), corresponding to 2–3 specimens per level. Although this sample size limits rigorous statistical characterization (e.g., reliability bounds), the fatigue life results show consistent trends with increasing load. Therefore, the S–N curves presented in this study illustrate the geometry-sensitive stress–life relationship rather than statistically validated design curves.

3.3 Crack Propagation Modes

Three dominant crack propagation modes were identified (see Fig. 12(a-c):

Mode 1 Crack initiates and propagates entirely within the copper layer—associated with uniform fillet morphology and strong interfacial bonding.

Mode 2 Crack initiates in copper, redirects to SS–Cu interface, then propagates into STS—suggests internal defects or locally weakened regions.

Mode 3 Crack initiates directly at SS–Cu interface near joint edge—correlated with non-uniform fillet distribution. These failure modes are qualitatively similar to those observed by Jöckel et al. [39] in conventional peel specimens, where cracks initiated from initial defects in the fillet region and propagated either intergranularly through the brazing material or along the interface. However, the ultra-thin joints exhibited predominantly Mode 1 behavior (copper-confined propagation) due to the absence of macroscale initial defects, suggesting that defect-free ultra-thin joints follow more predictable failure paths.

The occurrence frequency of each crack propagation mode observed at different applied load levels is summarized in Table 3.

The observed transition from Mode 1 dominance at lower loads to increased occurrence of Mode 2 and Mode 3 at higher loads indicates that crack propagation behavior is governed by the interplay between applied stress and local

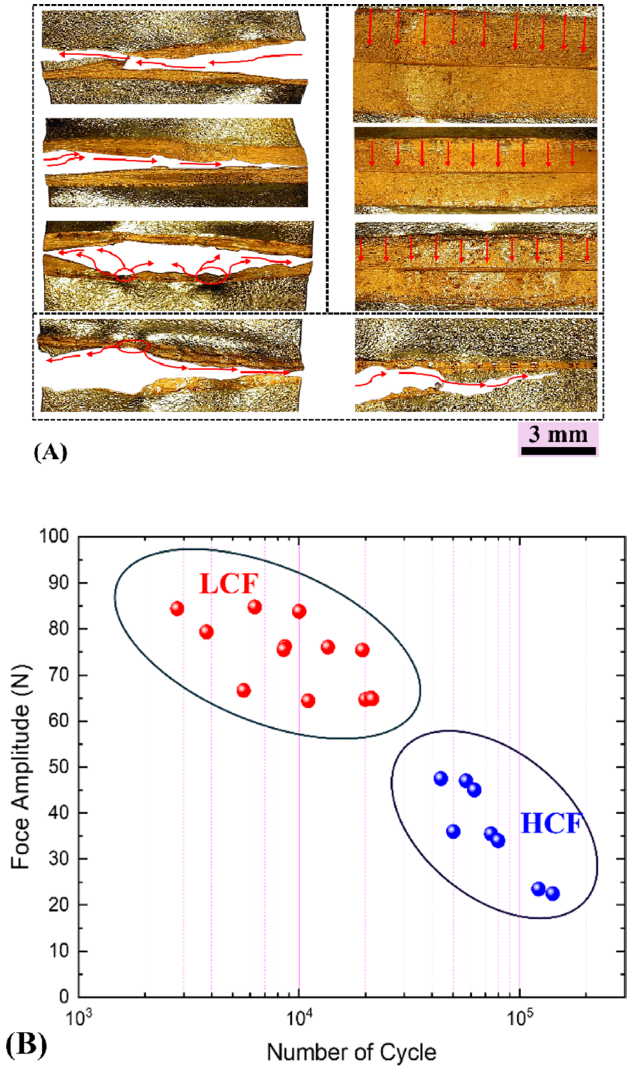

Fig. 11 (**A**) Crack initiation point and propagation morphology, (**B**) fatigue life data showing strong inverse relationship between maximum peel force and cycles to failure

geometry. As the load increases, stress concentration at the fillet and interface becomes sufficient to alter crack paths, promoting interface-involved failure modes. Consistent with Table 3, Mode 1 dominates at lower loads, whereas Mode 2 becomes more prevalent with increasing load, and Mode 3 appears only occasionally, indicating increased susceptibility to interface-related crack initiation.

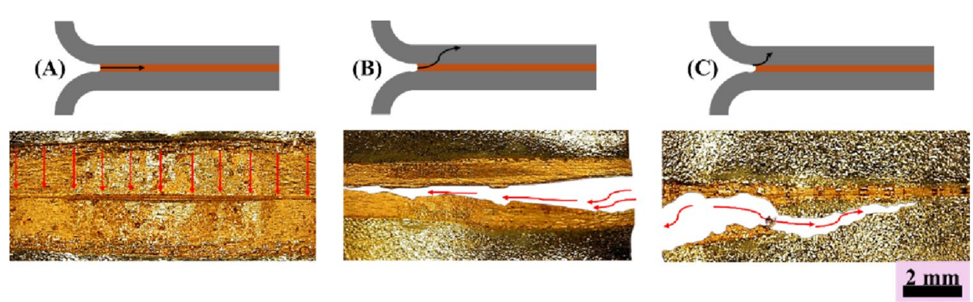

Fig. 12 Crack propagation modes: (**A**) Mode 1-copper-confined propagation, (**B**) Mode 2-copper to interface to STS, (C) Mode 3-interface-initiated propagation to STS

Table 3 Occurrence of crack propagation modes observed at different applied load levels

Load level (*N*)	Number of specimens	Mode 1	Mode 2	Mode 3
50	2	2	0	0
75	3	2	1	0
100	3	2	1	0
150	5	2	2	1
175	5	2	2	1
200	4	1	2	1

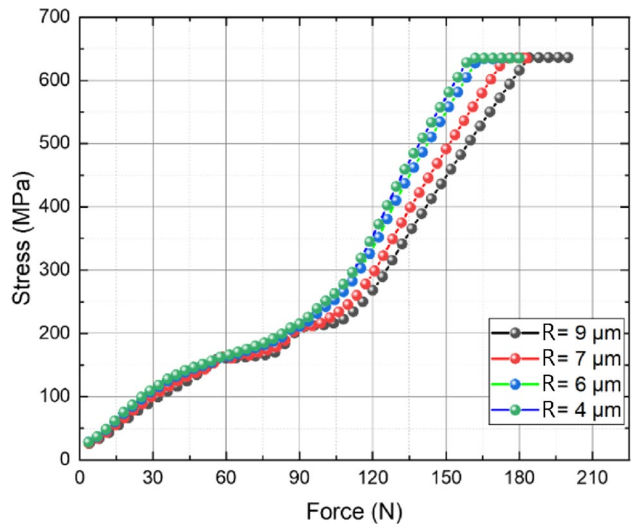

Fig. 13 Stress–force relationships for different fillet radii, showing load-dependent amplification of geometry effects in the plastic regime

3.4 Stress vs. Force Relationships and S-N Curves

Figure 13 presents FE-derived stress vs. force relationships at the fillet region. The load-dependent geometry effect is significant:

Near-yield regime (F_{max} ≈ 90 N): 217 MPa for $R = 4$ μm versus 205 MPa for $R = 9$ μm (6% difference), and **Plastic regime (F_{max} = 150 N)**: 580 MPa for $R = 4$ μm versus 448 MPa for $R = 9$ μm (30% difference).

This load-dependent amplification of geometry effects is consistent with findings by Jöckel et al. [39], who reported that the local stress approach successfully rationalized fatigue data across different fillet geometries. However, the magnitude of the effect is substantially larger in ultra-thin joints due to the micro-scale fillet dimensions. This result

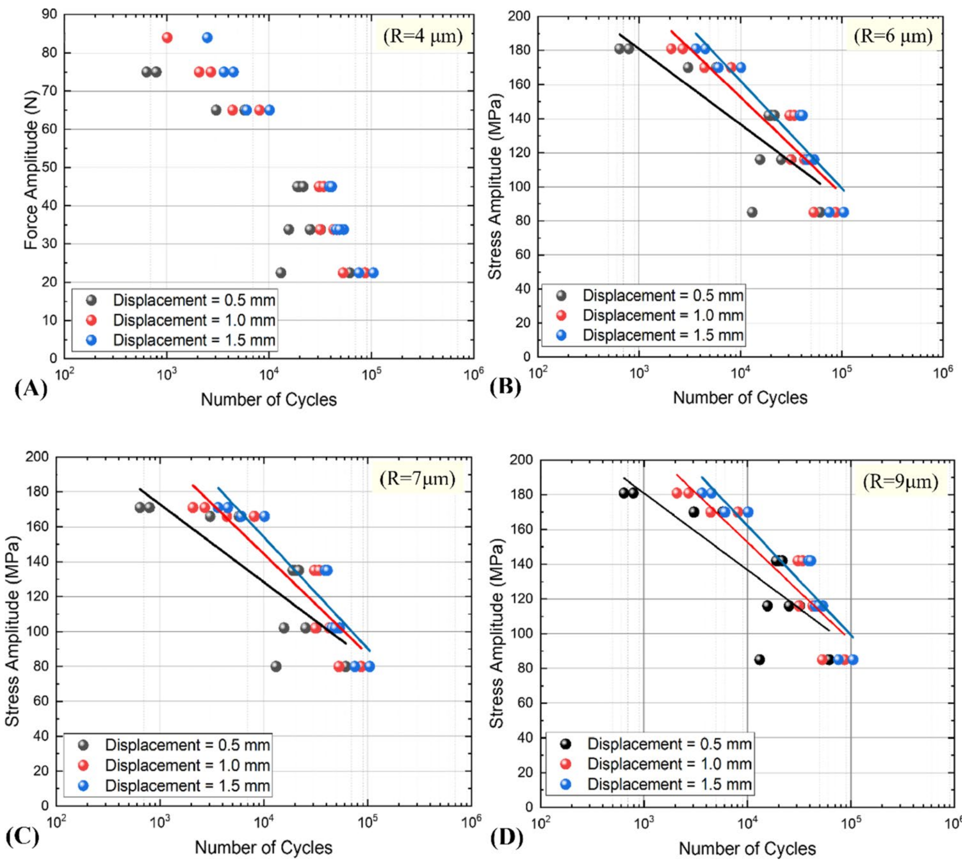

Fig. 14 (**A**) Experimental force–life (F–N) data, (**B**–**D**) stress–life (S–N) curves at different displacement levels for fillet radii of 6, 7, and 9 µm

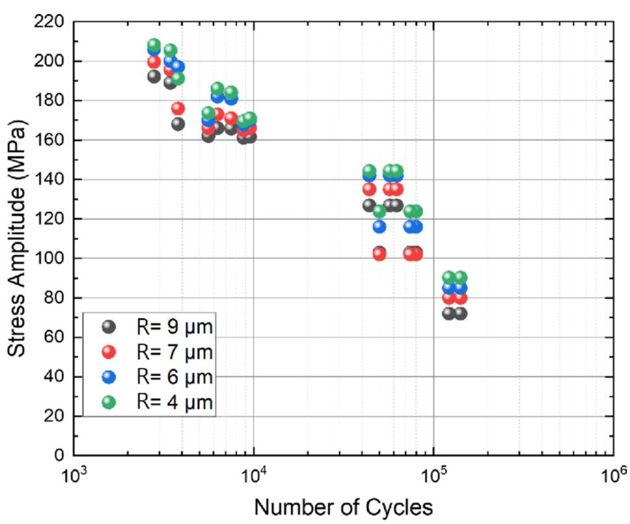

Fig. 15 Stress vs. life (S-N) curves demonstrating fillet radius effect: larger radii reduce local stress and improve fatigue resistance

demonstrates that geometric effects become increasingly dominant in the plastic regime, where small variations in fillet radius lead to significant differences in local stress. Consequently, fatigue behavior in ultra-thin joints is sensitive to micro-scale geometric features under elevated loading conditions.

Figures 14 and 15 present the S-N curves showing systematic fillet radius dependence. The stress-based framework successfully captures geometric sensitivity not evident in force-based evaluation, similar to the local stress approach validated by Jöckel et al. [39] for conventional brazed joints. This confirms that local stress at the fillet is the governing parameter for fatigue failure. These results indicate that force-based evaluation alone is insufficient to capture the geometry-dependent fatigue behavior in ultra-thin joints.

Figure 16 shows crack growth behavior exhibiting two stages: prolonged low-rate growth followed by exponential acceleration. This two-stage behavior is consistent with fatigue crack growth in conventional brazed joints, where Jöckel et al. [39] reported that crack initiation occupied approximately 42% of total fatigue life in shear specimens. However, in ultra-thin peel specimens, the transition to rapid propagation appears more abrupt, likely due to the limited ligament area available for stable crack growth. The initial low-rate growth stage corresponds to stable crack propagation within the copper layer, where plastic deformation redistributes stress at the crack tip. The subsequent rapid acceleration stage occurs when the remaining ligament becomes insufficient to sustain the applied load, leading to unstable crack propagation and final failure.

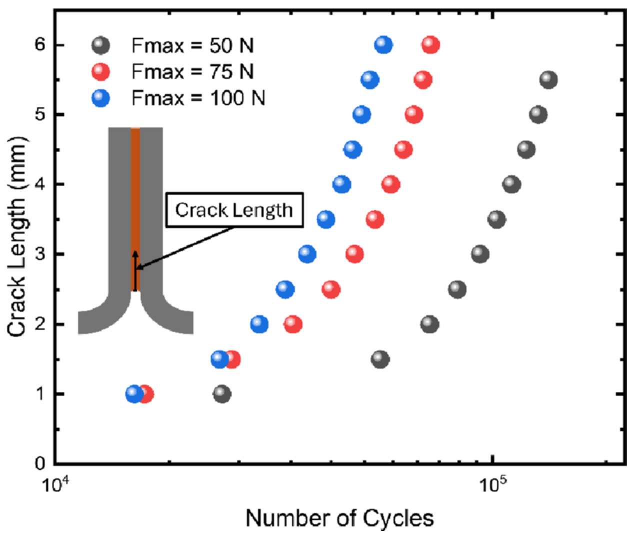

Fig. 16 Crack growth response showing two-stage behavior: prolonged low-rate growth followed by exponential acceleration preceding failure

4 Discussion

The present study reveals several key differences between ultra-thin and conventional brazed joint fatigue behavior: (1) Defect sensitivity: Jöckel et al. [39] reported that crack-like initial defects (up to 0.4 mm depth) had considerable influence on fatigue life in conventional joints. In contrast, the ultra-thin joints in this study exhibited excellent bonding quality without such defects, indicating that the vacuum brazing process produces higher-quality joints at the micro-scale, possibly due to more uniform heat distribution and filler flow in thinner assemblies. (2) Fillet geometry scale: The fillet radii in conventional studies (0.26–2.76 mm in [39], comparable scale in [10, 16]) are 30–300× larger than those in ultra-thin joints (4–13 μm). This dramatic difference in geometric scale suggests that stress concentration mechanisms may differ fundamentally—while conventional fillets approximate continuum stress concentration factors, ultra-thin fillets approach the scale of individual grains, potentially introducing microstructure-geometry interactions. (3) Loading mode relevance: Previous studies [10, 16] primarily employed uniaxial tension or strain-controlled loading, which may not accurately represent PHE service conditions. The peel-mode loading in this study more directly replicates the Mode-I crack-driving forces at brazed joint fillets during pressure cycling, as emphasized by multiple investigators [12, 16, 39]. (4) Fatigue life ranges: Despite the differences in geometry and loading mode, the fatigue life ranges in this study (10^3~10^5 cycles) are comparable to those reported by Hayta and Kandemir [16] (10^3~10^5 cycles) and Hanželič et al. [10] (10^5~10^6 cycles for HCF). This suggests that the fundamental damage mechanisms, crack initiation at stress concentrations followed by propagation through the copper layer, are similar across scales, though governed by different geometric parameters. This consistency in fatigue life range and crack propagation behavior with previously reported experimental studies provides validation of the present results, confirming that the proposed experimental and numerical approach captures the essential fatigue mechanisms in brazed joints across different scales.

The combined results demonstrate that fatigue failure of ultra-thin brazed joints under peel loading is governed by local stress concentration at the fillet rather than applied force alone. This finding extends the conclusions of Jöckel et al. [39], who showed that local stress approaches successfully rationalized fatigue data for conventional brazed joints with various fillet geometries. The microstructural observations, excellent bonding without voids or intermetallic phases, establish that geometry, not material defects, governs fatigue behavior in well-manufactured ultra-thin joints. This has important implications: fatigue reliability can be significantly improved through brazing process control targeting fillet geometry, without requiring material changes. This interpretation is directly supported by the stress–force relationships shown in Fig. 13, where the effect of fillet radius increases from 6% near yield to 30% in the plastic regime. This result confirms that geometric effects become increasingly dominant as plastic deformation develops, providing a mechanistic basis for the observed fatigue trends. Furthermore, the agreement between the present stress-based trends and those reported for conventional brazed joints supports the validity of the local stress approach, while extending its applicability to ultra-thin configurations.

The two fatigue regimes reflect fundamentally different damage mechanisms. In HCF (50~100 N), the copper layer accommodates cyclic deformation through plastic strain, enabling stable crack growth and extended life (10^4~10^5 cycles). In LCF (150~200 N), loads exceed yield, pronounced stress amplification at the fillet drives rapid failure (10^3~10^4 cycles). This transition is analogous to the elastic-plastic transition observed in conventional fatigue testing, but occurs at the micro-scale fillet rather than in bulk material.

Based on comparison with existing literature and the present experimental-numerical results, the following design guidelines are proposed for ultra-thin brazed joints: (1) Maximize fillet radii within manufacturing constraints, the present study shows that increasing fillet radius from 4 to 9 μm reduces local stress by 6% near yield and 30% in the plastic regime. (2) Ensure fillet uniformity to prevent localized stress concentrations that promote Modes 2/3 failure, as non-uniform fillets redirect cracks toward interfaces. (3) Use peel-mode testing for fatigue characterization of PHE joints, as this loading mode more accurately represents service conditions than uniaxial tension or lap-shear testing. (4) Apply stress-based (not force-based) criteria for fatigue assessment, as demonstrated by both this study and previous work on conventional joints [39]. (5) Consider thickness-dependent mechanisms when extrapolating fatigue data from conventional to ultra-thin joints, as the micro-scale fillet geometry introduces unique stress concentration effects. This is further evidenced by the S-N curves (Figs. 14 and 15), where stress-based evaluation reveals clear geometric sensitivity that is not captured in force-based representations, reinforcing the importance of local stress as the governing fatigue parameter.

One limitation of the present study is associated with the determination of material properties of the copper interlayer. Due to the ultra-thin thickness of the filler layer and its confinement between stainless steel sheets, direct measurement of its local mechanical properties after brazing is experimentally infeasible. Therefore, an inverse calibration approach based on the force–displacement response of brazed multilayer specimens was adopted to determine the effective constitutive behavior. While this approach captures the overall mechanical response of the joint, the calibrated properties should be interpreted as an effective representation for the present configuration, and may not fully account for local variations within the fillet region. Further validation using advanced micro-scale characterization techniques would help improve the accuracy and generality of the material model.

5 Conclusions

This study presents, to the best of the authors' knowledge, the first systematic characterization of peel mode fatigue behavior in ultra-thin 50 µm copper brazed 316 L stainless steel joints through an integrated experimental and numerical framework, with comprehensive comparison to existing literature on conventional brazed joints. It addresses the combined effects of ultra-thin sheet thickness, micro-scale fillet geometry, and peel mode loading, which are not simultaneously considered in existing studies. The main conclusions are summarized as follows:

1. Microstructural characterization confirmed that the brazed joints exhibit continuous copper interlayers with micro-scale fillet radii of approximately 4 to 7 µm and defect free bonding. This distinguishes them from conventional brazed joints where crack-like initial defects are often present, indicating fundamentally different defect sensitivity at the ultra-thin scale.
2. Monotonic and cyclic peel testing demonstrated that fatigue behavior is governed by Mode I loading at the fillet rather than applied force. Two distinct regimes were identified. High cycle fatigue in the range of 50 to 100 N corresponds to stable crack growth within the copper layer with lives on the order of 10^4 to 10^5 cycles, while low cycle fatigue in the range of 150 to 200 N is dominated by plastic deformation and rapid failure with lives on the order of 10^3 to 10^4 cycles.
3. Finite element analysis successfully captured the local stress distribution at the fillet region and confirmed that stress concentration is strongly dependent on micro-scale fillet geometry under peel loading conditions, providing a consistent mechanistic basis for the observed fatigue behavior.
4. A geometry sensitive stress-life relationship was established, showing that the influence of fillet radius is strongly load dependent, increasing from approximately 6% near yield to 30% in the plastic regime. This demonstrates that geometric effects become increasingly dominant as plastic deformation develops and extends the applicability of the local stress approach to ultra-thin joints.
5. Comparison with existing studies showed that although fatigue life ranges are comparable to those reported for conventional joints, the governing mechanisms differ due to micro-scale geometry and peel mode loading. This agreement with previous experimental observations validates the present approach while highlighting the thickness dependent nature of fatigue behavior.

Overall, the results demonstrate that fatigue performance in ultra-thin brazed joints is governed by local stress concentration at micro-scale fillet features rather than applied force alone. These findings emphasize the critical importance of geometry control and stress based evaluation for the reliable design of fatigue critical plate heat exchanger joints.

Acknowledgements This research was supported by Korea Basic Science Institute (National research Facilities and Equipment Center) grant funded by the Ministry of Education. (grant No. 2021R1A6C101A449) and the National Research Foundation of Korea(NRF) grant funded by the Korea government(MSIT)(No. RS-2023-NR076859).

Author Contribution Melkamu Tadesse Getachew: Conceptualization, Methodology, Investigation, Software, Formal analysis, Validation, Visualization, Writing – original draft, Writing- review & editing.

Hong-Seok Kim: Conceptualization, Methodology, Investigation, Formal analysis, Visualization, Writing – review & editing. Seokyoung Ahn: Resources. Sang-Hu Park: Supervision, Project administration, Funding acquisition, Writing – review & editing.

Data availability Data supporting this study are available from the corresponding author upon reasonable request.

Declarations

Competing Interests The authors declare no known competing financial interests or personal relationships that could have influenced this work.

References

1. Ma, H., Cai, W., Yao, Y., & Jiang, Y. (2016). Investigation on stress characteristics of plate-fin structures in the heat-up process of LNG heat exchangers. *Journal of Natural Gas Science and Engineering*, *30*, 256–267. https://doi.org/10.1016/j.jngse.2016.02.029
2. Ge, L., Jiang, W., Wang, Y., & Tu, S. T. (2018). Creep–fatigue strength design of plate-fin heat exchangers by a homogeneous method. *International Journal of Mechanical Sciences*, *146–147*, 221–233. https://doi.org/10.1016/j.ijmecsci.2018.07.021
3. Li, B., Guo, S., Cai, B. H., & Wang, B. (2019). Design and fatigue analysis of high-pressure shell-and-plate heat exchangers. *IOP Conference Series: Earth and Environmental Science* 233, 052025. https://doi.org/10.1088/1755-1315/233/5/052025
4. Pelliccione, A. S., Sant'Anna, R., Siqueira, M. H. S., Ribeiro, A. F., Ramos, J. E., Silva, O. P., & Pimentel, M. F. (2019). Failure analysis of a titanium plate heat exchanger under mechanical fatigue. *Engineering Failure Analysis*, *105*, 1172–1188. https://doi.org/10.1016/j.engfailanal.2019.07.059
5. Jeong, H. S., Cho, J. R., Jeon, J. W., & Park, S. H. (2014). Investigation into structural reliability of a brazed part in cross-corrugated plates. *International Journal of Precision Engineering and Manufacturing*, *15*, 251–258. https://doi.org/10.1007/s12541-014-0332-y
6. Bobič, M., Gjerek, B., Golobič, I., & Bajsić, I. (2020). Dynamic behaviour of a plate heat exchanger: Influence of temperature disturbances and flow configurations. *International Journal of Heat and Mass Transfer*, *163*, 120439. https://doi.org/10.1016/j.ijheatmasstransfer.2020.120439
7. Ma, H., Wang, J., Chen, H., Bai, J., Cai, W., Wang, S., & Ding, R. (2024). Numerical investigation on thermal fatigue damage mechanisms of head structures in aluminum plate-fin heat exchangers. *Journal of Materials Engineering and Performance*, *33*, 13670–13684. https://doi.org/10.1007/s11665-023-08924-z
8. Kim, C. S., Kim, H. J., Cho, J. R., Park, S. H., & Ha, M. Y. (2016). Manufacturing and mechanical evaluation of cooled cooling air heat exchangers for aero engines. *International Journal of Precision Engineering and Manufacturing*, *17*, 1195–1200. https://doi.org/10.1007/s12541-016-0143-4
9. Mizokami, Y., Igari, T., Kawashima, F., Sakakibara, N., Tanihira, M., Yuhara, T., & Hiroe, T. (2013). Development of structural design procedures for plate-fin heat exchangers in HTGR systems. *Nuclear Engineering and Design*, *255*, 248–262. https://doi.org/10.1016/j.nucengdes.2012.09.013
10. Hanželič, B., Kralj, J., Bončina, T., Nečemer, B., Kramberger, J., Satošek, R., & Glodež, S. (2024). Fatigue behaviour of brazed joints for heat exchangers. *Materials*, *17*, 479. https://doi.org/10.3390/ma17020479
11. Cho, H. C., Na, B. J., Ahn, C. H., Shin, B. S., Park, S. H., Son, C., Moon, H. S., & Go, J. S. (2015). Development of a pressure distribution measurement method for compact and complex heat exchangers. *Flow Measurement and Instrumentation*, *46*, 93–102. https://doi.org/10.1016/j.flowmeasinst.2015.10.008
12. Chen, H., Li, N., Wei, X., Liu, S., & Ling, X. (2023). Effect of brazing fillet geometry on microstructure and mechanical properties of vacuum-brazed stainless steel joints. *Metals*, *13*, 1369. https://doi.org/10.3390/met13081369
13. Remešová, M., Klakurková, L., Skalka, P., Gejdoš, P., Juliš, M., & Čelko, L. (2025). Failure analysis of copper heating blocks designed for brazing sheets. *Engineering Failure Analysis*, *178*, 109718. https://doi.org/10.1016/j.engfailanal.2025.109718
14. Zhang, H. Y., Xu, W., Zhu, T. Y., Qu, S., Dong, C., Wang, X. G., & Zhang, Z. F. (2023). Standstill corrosion of BNi-2/316L brazed joints in a Stirling engine. *Engineering Failure Analysis*, *146*, 107150. https://doi.org/10.1016/j.engfailanal.2023.107150
15. Kim, H. S., Getachew, M. T., Ahn, S. Y., & Park, S. H. (2025). Comparison of copper filler infiltration behavior in ultra-thin stainless steels (304, 304L, and 316L) during brazing. *Journal of Materials Research and Technology*, *39*, 3737–3747. https://doi.org/10.1016/j.jmrt.2025.10.032
16. Hayta, Y., & Kandemir, S. (2025). Fatigue assessment of copper-brazed stainless-steel joints for plate heat exchangers. *Fatigue & Fracture of Engineering Materials & Structures*, *48*, 725–737. https://doi.org/10.1111/ffe.14509
17. Carter, P., Carter, T. J., & Viljoen, A. (1996). Failure analysis and life prediction of a large, complex plate-fin heat exchanger. *Engineering Failure Analysis*, *3*, 29–43.
18. Luu, V. T., Dinh, T. K. A., Das, H., Kim, J. R., Hong, S. T., Sung, H. M., & Han, H. N. (2018). Diffusion enhancement during electrically assisted brazing of ferritic stainless steels. *International Journal of Precision Engineering and Manufacturing – Green Technology*, *5*, 613–621. https://doi.org/10.1007/s40684-018-0063-0
19. Kang, S. H., Park, S. H., Min, J. K., Cho, J. R., & Ha, M. Y. (2013). Evaluation of mechanical integrity of brazed joints in tube-type heat exchangers considering local material properties. *Proceedings of the Institution of Mechanical Engineers Part C*, *227*, 420–433. https://doi.org/10.1177/0954406212463845
20. Mahajan, H. P., McKillop, S., Keating, R., & Hassan, T. (2022). Proposed material properties, allowable stresses, and design curves for diffusion-bonded Alloy 800H under ASME Section III Division 5. *Journal of Pressure Vessel Technology*, *144*, 041502. https://doi.org/10.1115/1.4054073
21. Mahajan, H. P., Lima, L. M. A., & Hassan, T. (2022). Mechanical and microstructural performance of diffusion-bonded Alloy 800H for very-high-temperature nuclear service. *Journal of Engineering Materials and Technology*, *144*, 031006. https://doi.org/10.1115/1.4052825
22. Jiang, W., Gong, J. M., & Tu, S. T. (2011). Fatigue life prediction of stainless steel plate-fin structures using an equivalent homogeneous solid method. *Materials & Design*, *32*, 4936–4942. https://doi.org/10.1016/j.matdes.2011.05.048
23. Martins, G. S. M., da Silva, R. P. P., Beckedorff, L., Monteiro, A. S., de Paiva, K. V., & Oliveira, J. L. G. (2020). Fatigue performance evaluation of plate and shell heat exchangers. *International Journal of Pressure Vessels and Piping*, *188*, 104237. https://doi.org/10.1016/j.ijpvp.2020.104237
24. Lee, C. W., Lee, S. J., Kim, I. J., & Kim, J. (2024). Detection of joint defects in copper tube induction-brazed regions using infrared thermal imaging and CNN algorithms. *International Journal of Precision Engineering and Manufacturing*, *25*, 687–697. https://doi.org/10.1007/s12541-023-00944-y
25. Holländer, U., Wulff, D., Langohr, A., Möhwald, K., & Maier, H. J. (2020). Brazing in SiH_4-doped inert gases: An environmentally friendly production process. *International Journal of Precision Engineering and Manufacturing – Green Technology*, *7*, 1059–1071. https://doi.org/10.1007/s40684-019-00109-1
26. Jeong, H. S., Cho, J. R., Min, J. K., Ha, M. Y., & Park, S. H. (2019). Influence of geometric variables on structural characteristics of brazed cross-corrugated sinusoidal plates with secondary

corrugation. *Journal of Mechanical Science and Technology*, *33*, 1851–1859. https://doi.org/10.1007/s12206-019-0337-7
27. Ma, H., Jia, J., Ding, R., Luo, X., Peng, D., Hou, C., Wang, G., & Zhang, Y. (2022). Numerical investigation of fatigue life of aluminum brazed structures under low-temperature thermo-mechanical cyclic loading. *Engineering Failure Analysis*, *131*, 105918. https://doi.org/10.1016/j.engfailanal.2021.105918
28. Htut, T. T., Tanaka, S., Ma, D., Okada, J., Honnami, M., Shinoda, K., Abe, M., & Katayama, T. (2024). Fatigue fracture characteristics of duplex stainless steel STHE welded joints. *Engineering Failure Analysis*, *155*, 107763. https://doi.org/10.1016/j.engfailanal.2023.107763
29. Donnelly, E., Weafer, F. M., Connolley, T., McHugh, P. E., & Bruzzi, M. S. (2017). Size effects on microscale fatigue behaviour of 316L stainless steel. *International Journal of Fatigue*, *95*, 1–7. https://doi.org/10.1016/j.ijfatigue.2016.10.007
30. Song, M., Liu, X., & Liu, L. (2017). Size effects on mechanical properties and texture evolution of cold-rolled pure copper foils. *Materials*, *10*, 538. https://doi.org/10.3390/ma10050538
31. Saggu, M. H., Sheikh, N. A., Niazi, U. M., Irfan, M., Glowacz, A., & Legutko, S. (2020). Reliability analysis of fins in LNG plate-fin heat exchangers. *Energies*, *13*, 3624. https://doi.org/10.3390/en13143624
32. Griffith, A. A. (1921). The phenomena of rupture and flow in solids. *Philosophical Transactions of the Royal Society A*, *221*, 163–198. https://doi.org/10.1098/rsta.1921.0006
33. Radgolchin, M., & Anbarsooz, M. (2023). Fatigue failure of centrifugal compressor impellers: A comprehensive review. *Engineering Failure Analysis*, *153*, 107592. https://doi.org/10.1016/j.engfailanal.2023.107592
34. Jahangiri, M. R. (2011). Failure analysis of type 304 stainless steel tubes in heat exchangers of energy production plants. *Journal of Pressure Vessel Technology*, *133*, 041403. https://doi.org/10.1115/1.4003811
35. Fang, J. H., Xie, M., Yang, Y. C., Kozinov, S., Kuna, M., Roth, S., Fan, Z., Zhang, K., Liu, J., Wu, Y., Xing, A., Cheng, Q., & Li, Q. (2023). Interface strength investigation of 304 stainless steel/T2 copper T-type brazed joints using a cohesive zone model. *Materials Research Express*, *10*, 016517. https://doi.org/10.1088/2053-1591/acb252
36. Brely, L., Bosia, F., Pugno, N. M., Chen, H., Chen, S., & Kendall, K. (1975). Thin-film peeling: Elastic energy contribution. *Journal of Physics D: Applied Physics*, *8*, 1449–1456. https://doi.org/10.1088/0022-3727/8/13/005
37. Ma, H., Jia, J., Liu, Y., Luo, X., Hou, C., & Wang, G. (2023). Fatigue analysis of brazed structures in LNG heat exchangers under cryogenic conditions. *Science and Technology for Energy Transition*, *78*, 12. https://doi.org/10.2516/stet/2023002
38. Jöckel, A., Baumgartner, J., Tillmann, W., Bültena, J., Bobzin, K., Heinemann, H., & Erck, M. (2023). Local stress-based fatigue strength assessment of brazed joints considering seam quality. *Welding in the World*, *67*, 1833–1852. https://doi.org/10.1007/s40194-023-01524-4
39. Jöckel, A., Baumgartner, J., Tillmann, W., Bültena, J., Bobzin, K., Heinemann, H., Hebing, J., & Erck, M. (2022). Influence of brazing process and gap size on fatigue strength of shear and peel specimens. *Welding in the World*, *66*, 1941–1955. https://doi.org/10.1007/s40194-022-01304-6
40. ASTM D1002-10. (2010). *Standard test method for apparent shear strength of single-lap-joint adhesively bonded metal specimens by tension loading*. ASTM International.
41. Roylance, D. (2001). *Stress–strain curves*. Massachusetts Institute of Technology.